Petroleum Science 21 (2024) 2638–2649

Contents lists available at ScienceDirect

Petroleum Science

journal homepage: www.keaipublishing.com/en/journals/petroleum-science

Original Paper

Effect of low-speed waterjet pressure on the rock-breaking performance of unsubmerged cavitating abrasive waterjet

Chen-Xing Fan [a, b], Deng Li [a, b], Yong Kang [a, b, *], Hai-Tao Zhang [a, b]

[a] Hubei Key Laboratory of Waterjet Theory and New Technology, Wuhan University, Wuhan, 430072, Hubei, China
[b] School of Power and Mechanical Engineering, Wuhan University, Wuhan, 430072, Hubei, China

ARTICLE INFO

Article history:
Received 8 June 2023
Received in revised form
17 March 2024
Accepted 18 March 2024
Available online 20 March 2024

Edited by Jia-Jia Fei

Keywords:
Rock-breaking
Coaxial low-speed waterjet pressure
Abrasive waterjet
Cavitation
Unsubmerged environment

ABSTRACT

Unsubmerged cavitating abrasive waterjet (UCAWJ) has been shown to artificially create a submerged environment that produces shear cavitation, which effectively enhances rock-breaking performance. The shear cavitation generation and collapse intensity depend on the pressure difference between the intermediate high-speed abrasive waterjet and the coaxial low-speed waterjet. However, the effect of the pressure of the coaxial low-speed waterjet is pending. For this purpose, the effect of low-speed waterjet pressure on rock-breaking performance at different standoff distances was experimentally investigated, and the effects of erosion time and ruby nozzle diameter on erosion performance were discussed. Finally, the micromorphology of the sandstone was observed at different locations. The results show that increased erosion time and ruby nozzle diameter can significantly improve the rock-breaking performance. At different standoff distances, the mass loss increases first and then decreases with the increase of low-speed waterjet pressure, the maximum mass loss is 10.4 g at a low-speed waterjet pressure of 0.09 MPa. The surface morphology of cavitation erosion was measured using a 3D profiler, the increase in both erosion depth and surface roughness indicated a significant increase in the intensity of the shear cavitation collapse. At a low-speed waterjet pressure of 0.18 MPa, the cavitation erosion surface depth can reach 600 μm with a roughness of 127 μm.

1. Introduction

High-pressure waterjet is considered indispensable for rock-breaking in underground spaces such as rock-cutting (Ge et al., 2023; Grosso et al., 2021; Lu et al., 2015), coal bed methane extraction (Guo et al., 2019), and natural gas exploitation (Zhang et al., 2020). It is because of the advantages of low cost, high efficiency, dust-free, heat-free and pollution-free to the environment (Soyama, 2020). Efficient drilling and excellent rock-breaking performance are required in engineering applications. For this purpose, high-performance waterjets with strong destructive power have been developed based on continuous waterjets, including cavitation waterjet and abrasive waterjet.

As for the cavitating waterjet, the pressure waves, instantaneous high temperatures and micro-jets generated during the collapse of cavitation bubbles in the cavitating waterjet enhance the erosion ability. Watanabe et al. (2016) studied the structure of cavitation clouds by shadow imaging and accelerated pulse measurements. The cavitation cloud shows a periodic motion of development, contraction and separation in the cavitating waterjet. Peng K.W. et al. (2018) comprehensively evaluated the cavitation erosion potential of cavitating waterjet by measuring the cavitation erosion area. The results showed that the stagnation zone and the reflux zone above the impact wall are two key factors affecting the formation and variation of impact distribution patterns. Peng C. et al. (2018) clarified the relationship between cavitation clouds and cavitation erosion, the results show that the intensity of cavitation erosion is determined by cavitation cloud concentration and collapse intensity. Hutli et al. (2016) found that the cavitation number has a great influence on the cavitation intensity and the distribution of cavitation bubbles, the results show that mass loss, erosion rate and eroded area increase as the cavitation number decreases.

As for the abrasive waterjet, which formed by introducing abrasive particles into the waterjet greatly enhances the working

* Corresponding author. Hubei Key Laboratory of Waterjet Theory and New Technology, Wuhan University, Wuhan, 430072, Hubei, China.
E-mail address: kangyong@whu.edu.cn (Y. Kang).

https://doi.org/10.1016/j.petsci.2024.03.012

efficiency and impact ability. Xue et al. (2018) compared the erosion characteristics of abrasive waterjet and pure waterjet, demonstrating that abrasive waterjet has a more concentrated erosion area and a higher cutting efficiency. Wang et al. (2018) established a mathematical model of rock stress under the impact of abrasive waterjet, providing a new idea for revealing the microscopic mechanism of rock-breaking. Liu et al. (2020) used abrasive waterjet to assist conical picks for rock breaking, in order to reduce the cuttings resistance. Bruno Arab and Barreto Celestino (2020) presented a microscopic study of rocks impinged by abrasive waterjet, and found that the rock disaggregation depends on the rock type and its microstructure. Cha et al. (2021) utilized steel shot as an abrasive to evaluate its erosion performance and recovery characteristics, the results showed that the steel shot cut 40%–50% deeper than garnet.

Related studies have shown that the addition of cavitation bubbles to the abrasive waterjet enhances erosion ability by using the synergistic relationship between the bubbles and the abrasive particles. For example, Lv et al. (2019) conducted an experimental study using the interaction of laser-induced cavitation bubbles and abrasive particles. The results showed that the growth of cavitation can be induced by the abrasive particles, the rupture of cavitation bubbles leads to the increase of abrasive acceleration. Pan et al. (2020a) used a venturi structure to create a cavitation bubble, which accelerated the impact of abrasive particles on the workpiece, resulting in a 52% increase in material removal compared with that without cavitation bubbles.

Based on previous studies, cavitating waterjet is only generated in a submerged environment, which greatly limits the application. Soyama et al. (Soyama, 2007; Soyama et al., 2011) first proposed an artificially submerged cavitating waterjet, which provides a promising solution to release this limitation. They found that the low-speed waterjet was one of the key parameters affecting the erosion ability of cavitating waterjet, the residual stress caused by erosion is minimized by low-speed waterjet at pressure of 0.05 MPa. Subsequently, Marcon et al. (Marcon et al., 2016, 2018) consistently increased the pressure of the coaxial low-speed waterjet and found that the mass loss of the specimen increased and then decreased. The erosion ability is maximized when the low-speed waterjet velocity approaches 11 m/s and is independent of the high-speed waterjet velocity. In addition, it was found that increasing the diameter of the high-speed waterjet nozzle could significantly improve erosion ability. Furthermore, environmental pressure also has a significant effect on the cavitation erosion ability in the submerged state. Cai et al. (2021) investigated the effect of ambient pressure on pulsed cavitating waterjet, the results showed that the ambient pressure changed the Strohal number to modulate the frequency characteristics of the waterjet. The standoff distance at which the optimal erosion ability of the cavitating waterjet was obtained at different ambient pressures through the analysis of Pan et al. (2020b), the effective erosion distance became sharply smaller as the ambient pressure increased. Hutli et al. (2016) found that the ambient pressure can change the cavitation number of the waterjet and thus affect its erosion ability.

According to the above discussion, to generate cavitation bubbles in an unsubmerged environment and enhance erosion ability by using their synergistic effect with abrasive particles. A new type of waterjet called unsubmerged cavitating abrasive waterjet (UCAWJ) was proposed in this study. However, the application of UCAWJ for rock-breaking is rare, meanwhile, the effect of low-speed waterjet on rock-breaking performance is ambiguous. Hence, in this study, after determining the erosion time and ruby nozzle diameter, the erosion behavior of sandstone at different low-speed waterjet pressures and standoff distances is investigated to determine the optimal rock-breaking parameters. Finally, the breaking mechanism of the sandstone is analyzed by combining high-speed photography and the micro-morphology of the sandstone.

2. Experimental setup and procedures

2.1. Experimental setup

The schematic diagram and the photograph of the experimental setup are shown in Fig. 1. The experimental setup was mainly composed of an abrasive supply system, a jet generator, a nozzle injecting the UCAWJ, and an erosion test unit. Among them, the abrasive supply system consisted of an abrasive supply tank, an agitator, a peristaltic pump, and a flowmeter.

Pure water and the abrasive particles were well mixed according to a certain proportion and stored in the supply tank as abrasive slurry. To prevent abrasive deposition, a high-speed agitator kept stirring the slurry during the experiment. The slurry was transported to the nozzle by a peristaltic pump with adjustable displacement. The jet generator consisted of a water tank, a filter, a high-pressure pump, a low-pressure pump, a pressure gauge, a flowmeter, and a control valve. The pressure loss in the pipeline from the high-pressure pump to the nozzle was ignored, and the flowmeter was used to obtain the waterjet flow rate. The nozzle consisted of two concentric parts, the inner and outer part of the nozzle were for the high-speed abrasive waterjet and the coaxial low-speed waterjet, respectively. The erosion test unit consisted of a tank, a drain pipe, and a holder, the specimens were fixed on the holder to avoid displacement during the experiment.

The composition of the nozzle is shown in Fig. 2. As shown in Fig. 2(a), the nozzle was mounted on the *Z*-direction moving axis of the 3D moving platform to facilitate the adjustment of the standoff distance in subsequent experiments. The standoff distance is defined as the distance between the nozzle outlet and the specimen surface. Fig. 2(b) shows a schematic diagram of the nozzle, the ruby nozzle which shown in Fig. 2(c) was installed at the uppermost end of the nozzle as the inlet of the high-speed waterjet. The sudden change of the nozzle diameter can form a negative pressure area in the mixing chamber. Quartz sand with sizes between 160 and 220 mesh was used as the abrasive particles, which are sucked into the mixing chamber and mixed with the high-speed waterjet, then accelerated out of the bottom of the nozzle. The coaxial low-speed waterjet was set outside the high-speed abrasive waterjet, the bottom of the nozzle as shown in Fig. 2(d). The nozzle in this work was made of stainless steel.

2.2. Materials

As shown in Fig. 3, rectangular shaped sandstone specimens of 100 mm in length, 100 mm in width and 50 mm in height were prepared, the basic physical properties of the specimens are shown in Table 1.

2.3. Experiment procedure

By controlling the experimental variables, the effects of low-speed waterjet pressure, standoff distance, erosion time and the diameter of the ruby nozzle on rock-breaking performance were studied. The test variables and their value ranges are shown in Table 2. Other parameters are provided as follows: the pressure of high-speed abrasive waterjet is 50 MPa, the impingement angle is

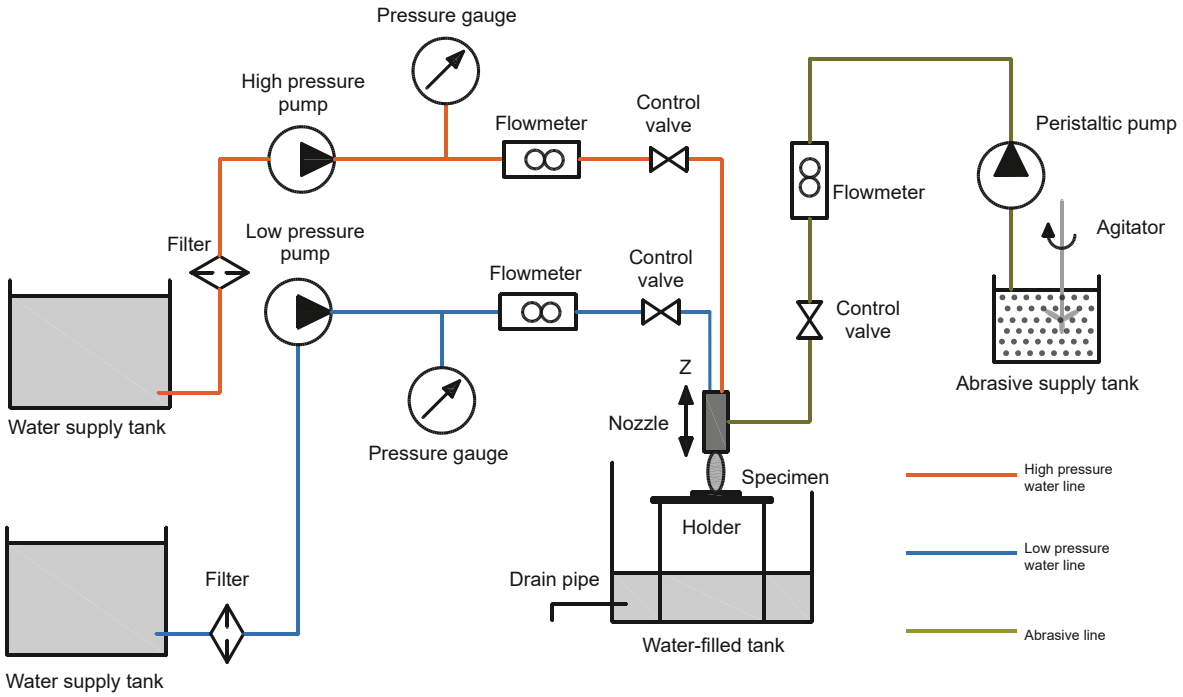

Fig. 1. Schematic diagram of experimental setup.

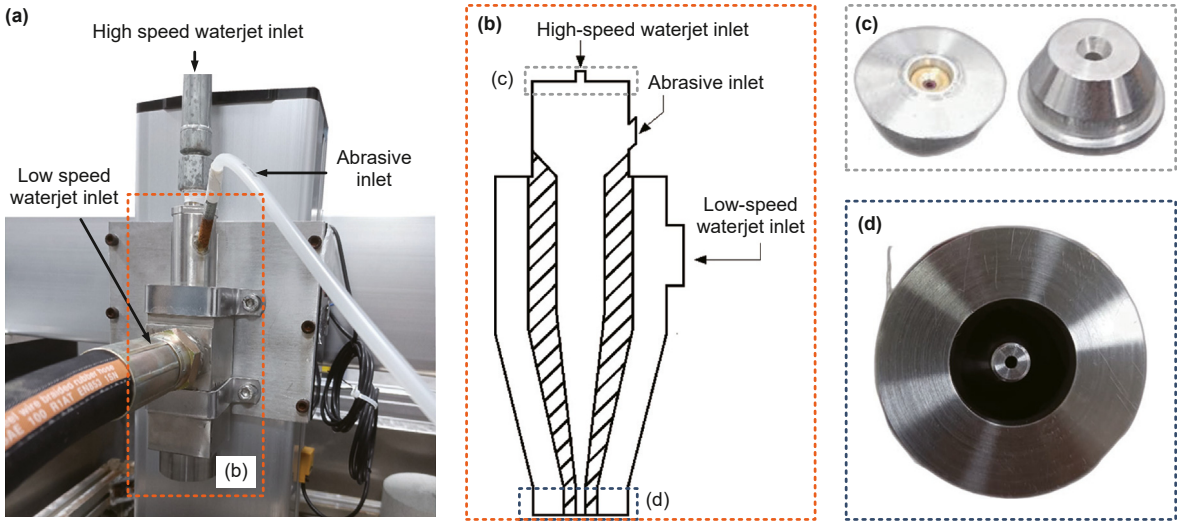

Fig. 2. Nozzle used in the experiment.

90°, the abrasive flow rate is 76 mL/min and the abrasive concentration is 3%.

The depth, area and mass loss of the erosion holes are used as indicators to evaluate rock-breaking performances and can be directly measured. The area of the erosion hole was calculated with help of the 3D profiler, erosion depth was measured by depth gauge and repeated three times. For the mass loss of sandstone, the sandstone was dried using an oven before and after the erosion to reduce the effect of the moisture contained in the sandstone on the measurement results. A scanning electron microscope (SEM) (Zeiss Sigma, Carl Zeiss AG Co. Ltd., Germany) was used to observe the surface characteristics, transient pictures of UCAWJ was captured with a high-speed camera (Phantom VEO710, Vision Research Inc., USA).

3. Results and discussion

3.1. Effect of erosion time and ruby nozzle diameter

Fig. 4 shows the schematic diagram of UCAWJ and the appearance of the sandstone after erosion. Abrasive particles are sucked into the negative pressure area, which is formed by the high-speed waterjet in the mixing chamber, where the abrasive particles are mixed with the high-speed waterjet and subsequently accelerated. Coaxial low-speed waterjet is applied externally to the high-speed waterjet, shear cavitation is generated in the contact boundary of the above two types of waterjets. Obvious erosion holes formed on the sandstone surface after erosion of the UCAWJ. The middle of the erosion area shows a deeper crater, mainly caused by high-speed

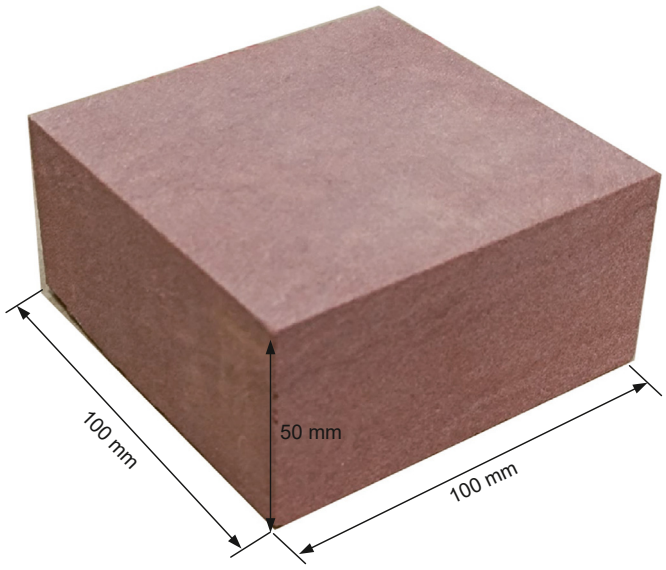

Fig. 3. Photograph of sandstone.

Table 1
Physical and mechanical properties of sandstone samples.

Properties	Value
Bulk density, g/cm^3	2.32
Uniaxial compressive strength, MPa	37
Tensile strength, MPa	2.4
Modulus of elasticity, GPa	3.44
Longitudinal wave velocity, m/s	2708

Table 2
Test variables and values.

Parameters	Values				
Erosion time, s	30	75	95	120	165
Ruby nozzle diameter, mm	0.5	0.6	0.7	0.8	1
Low-pressure waterjet, MPa	0.03	0.06	0.09	0.14	0.18
Standoff distance, mm	8	14	20	26	

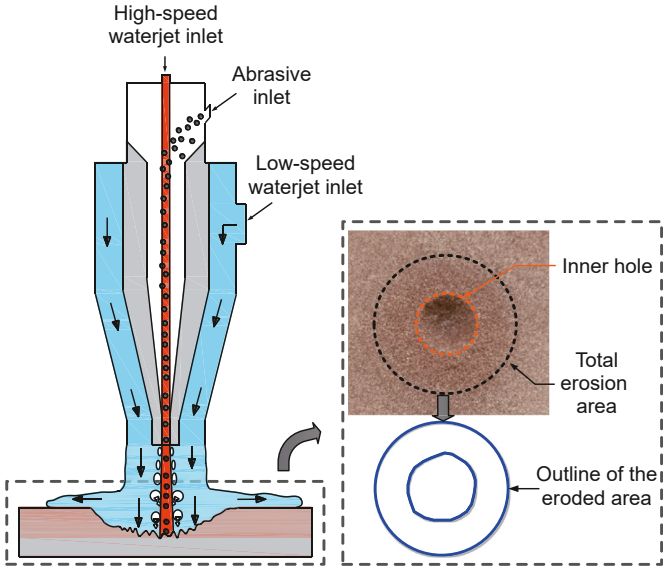

Fig. 4. Schematic diagram of UCAWJ and erosion appearance.

abrasive waterjet. The outer ring is formed under the erosion of shear cavitation, with an uneven outer appearance on the surface.

Predictably, the increase in erosion time and ruby nozzle diameter can improve the rock-breaking performance, but the proper of parameters for this study was selected with uncertainty. Fig. 5 shows the erosion appearance of sandstone with time and ruby nozzle diameter at high-speed abrasive waterjet pressure of 50 MPa, low-speed waterjet pressure of 0.09 MPa and standoff distance of 20 mm. As shown in Fig. 5(a), the appearances of the inner erosion holes are regular and close to circular, at an erosion time of 30 s, marks of erosion by cavitation bubbles could be observed on the sandstone surface. As shown in Fig. 5(b), the appearance of the erosion holes varies significantly at different diameters of the ruby nozzle. Slight erosion marks are observed when the ruby nozzle is 0.5 mm, the more obvious cavitation erosion area is obtained when the ruby nozzle is 0.6 mm. Internal erosion holes begin to become obvious when the ruby nozzle is larger than 0.7 mm and are more clearly characterized as the diameter increases.

As shown in Fig. 6(a), when the diameter of the ruby nozzle is 0.5 mm, the color of the high-speed waterjet is relatively light. Besides, the cavitation bubbles generated have basically collapsed at the standoff distance of 20 mm, resulting in weak erosion on the surface of the sandstone, which is similar to Fig. 5(b). As the ruby nozzle diameter increases, the high-speed waterjet is observed more clearly, the length of the resulting cavitation cloud increases. When the ruby nozzle diameter is 1 mm, the higher flow rate of high-speed waterjet and low-speed waterjet shear each other, resulting in more shear cavitation. Moreover, with the increase of flow rate, the length of the high-speed waterjet attenuation also increases, and the impact energy reaching the surface of the sandstone is larger, resulting in sandstone particles being more easily eroded. This result can well illustrate the erosion morphology of sandstone in Fig. 5(b).

To quantitatively characterize erosion performance over time, erosion area equivalent diameter, depth and mass loss were measured. As shown in Fig. 7(a), the equivalent diameter of the eroded area becomes larger and more sandstone is eroded as time increases. As shown in Fig. 7(b), erosion depth and mass loss increase significantly with time. The depth of erosion increases approximately linearly, reaching 4.85 mm at an erosion time of 165 s, with a similar trend in mass loss, reaching 10.13 g. For the consideration of experimental equipment parameters, an erosion time of 120 s will be employed in the subsequent experiments.

Similarly, the effect of ruby nozzle diameter was explored. As shown in Fig. 8, the erosion area total diameter continues to increase within 0.7 mm of the ruby nozzle. While the diameter of the ruby nozzle is greater than 0.7 mm, the total diameter of the erosion area changes more gently. The diameter of the inner ring erosion hole is continuously getting larger, this is due to the increase in the diameter of the ruby nozzle, which enhances the penetration ability of the waterjet. In this study, the ruby nozzle diameter is smaller than 0.7 mm, and the momentum of the high-speed waterjet decreases sharply, it is difficult to cause effective erosion of the sandstone before reaching the sandstone surface. While the ruby nozzle is larger than 0.7 mm, the momentum of the high-speed abrasive waterjet increases, after the exchange of momentum with the low-speed waterjet it is still able to cause significant erosion holes on the sandstone surface. As shown in Fig. 8(b), both erosion depth and mass loss increase sharply with increasing the diameter of the ruby nozzle. The results show that increasing the diameter of the ruby nozzle can significantly improve the rock-breaking performance. The diameter of the ruby nozzle chosen for subsequent experiments is 0.8 mm for the consideration of equipment parameters.

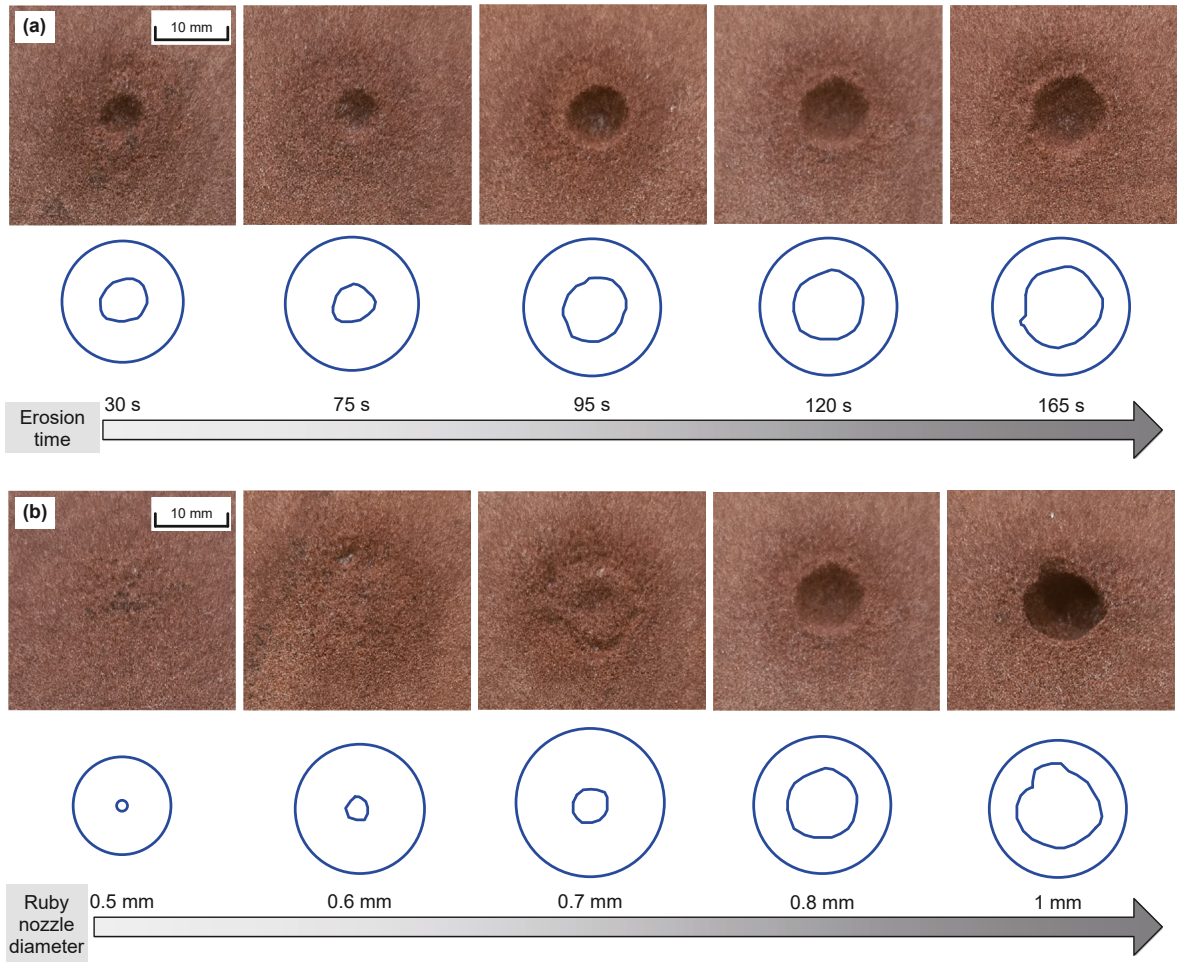

Fig. 5. Erosion hole appearance at different (**a**) erosion times and (**b**) ruby nozzle diameter.

3.2. Effect of low-speed waterjet pressure

For UCAWJ, the pressure of the low-speed waterjet is identified as an important parameter affecting the erosion performance. For this reason, shown in Fig. 9, the erosion hole appearance of the sandstone surface is demonstrated at standoff distance of 20 mm. The deeper but slightly smaller diameter of the inner erosion holes and no obvious cavitation erosion areas are observed on the sandstone surface at low-speed waterjet pressure of 0.03 MPa. Obvious cavitation erosion can be observed when the pressure of the low-speed waterjet gradually increases.

The trends of total diameter, inner erosion hole diameter, erosion depth and mass loss at different standoff distances under different low-speed waterjet pressures are shown in Fig. 10. As shown in Fig. 10(a), the total diameter of the eroded area increases and then decreases with increasing low-speed waterjet pressure. It can be observed that the total diameter of the eroded area is minimum at standoff distance of 8 mm. According to previous studies in the literature (Zelenak et al., 2022; Zheng et al., 2022), an increase in the standoff distance and the divergence of the waterjet leads to an increase in the eroded area. However, the diameter of the erosion area is generally larger at standoff distance of 20 mm compared with standoff distance of 26 mm. As shown in Fig. 10(b), the trend in the diameter of the inner erosion holes is similar to the total diameter. The erosion depth decreases with increasing low-speed waterjet pressure at different standoff distances as shown in Fig. 10(c). The erosion depth at smaller standoff distances is significantly superior compared with larger standoff distances. Meanwhile, the erosion depth decreases with the increase of low-speed waterjet pressure. Moreover, mass loss is a key indicator of rock-breaking performance, as shown in Fig. 10(d), the mass loss increases with the low-speed waterjet pressure and then decreases. Reaches a maximum value of 10.4 g at low-speed waterjet pressure of 0.09 MPa and standoff distance of 20 mm. In addition, the maximum mass loss is observed when the standoff distance is 20 mm at different low-speed waterjet pressure, the second largest mass loss is when the standoff distance is 8 mm. This indicates that there are two extreme values in mass loss, in the subsequent analysis, the erosion performance of the sandstone at standoff distance of 20 mm is mainly considered.

In terms of erosion area diameter, an increase in standoff distance and waterjet beam divergence will result in a larger erosion area, which can be observed in Fig. 10(b). But an increase in standoff distance may also cause the shear cavitation bubbles to collapse before they erode the sandstone, resulting in a reduced erosion area, which can be obtained in Fig. 10(a). For the erosion depth, the increased standoff distance allows for more dynamic energy exchange between the high-speed abrasive waterjet and the low-speed waterjet, the energy of the high-speed abrasive waterjet decays severely and the erosion depth decreases. In addition, the increased pressure of the low-speed waterjet, will further impede the high-speed abrasive waterjet, making the reduction of the erosion depth. Furthermore, mass loss depends mainly on the inner erosion holes and the outer ring cavitation erosion area. At standoff

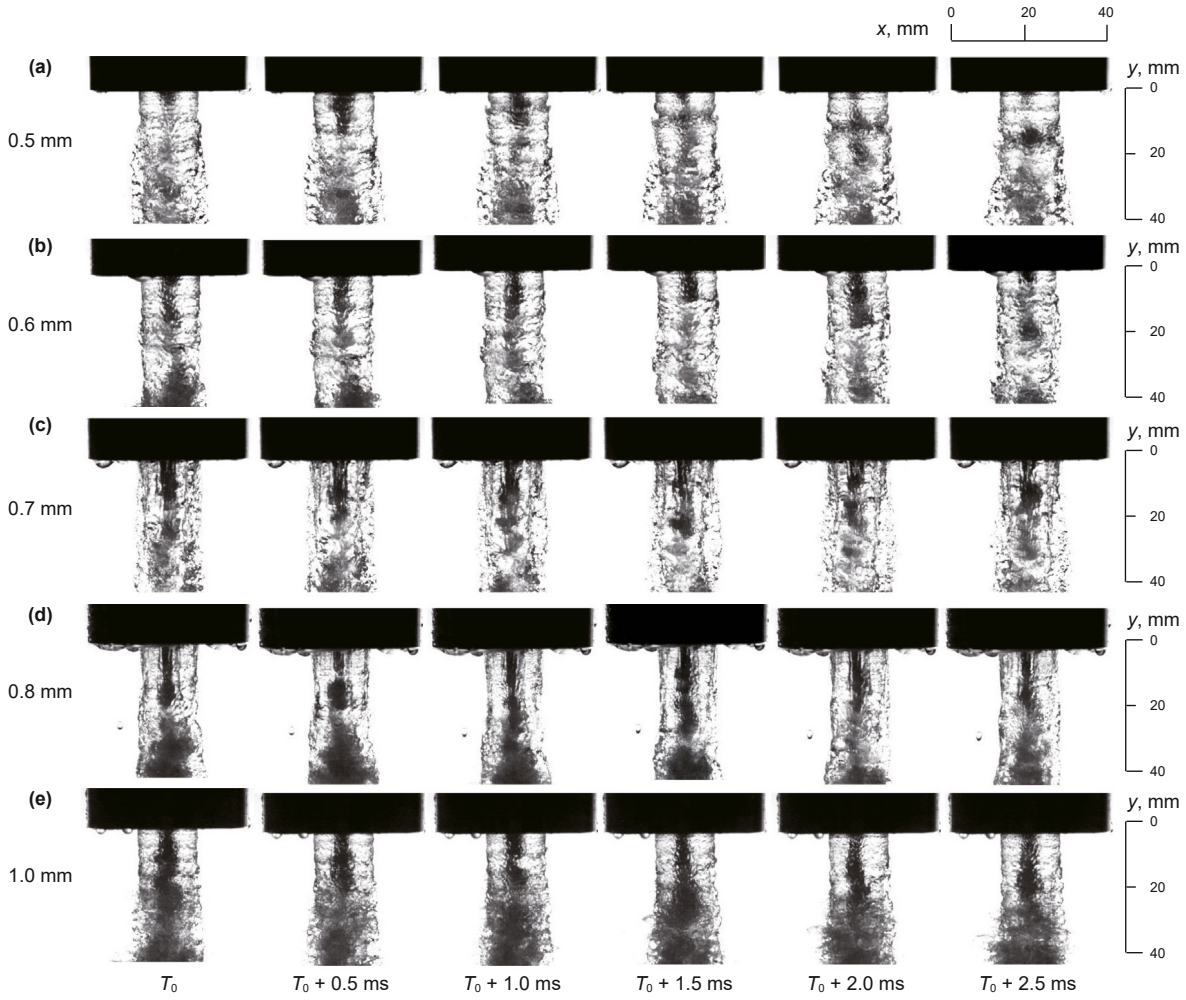

Fig. 6. Transient pictures of UCAWJ at different ruby nozzle diameters.

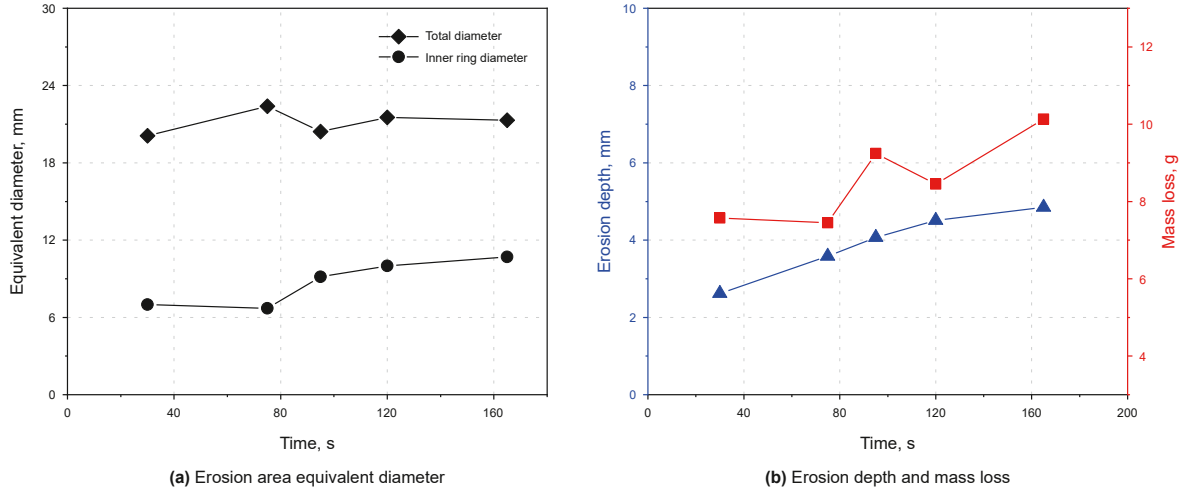

(a) Erosion area equivalent diameter

(b) Erosion depth and mass loss

Fig. 7. Rock-breakage performances of UCAWJ with various erosion times.

distance of 8 mm, the mass loss is mainly caused by abrasive waterjet erosion. At standoff distance of 20 mm, the mass loss due to abrasive waterjet erosion decreases, but the enhanced cavitation erosion can cause more sandstone to be eroded, which is the reason for the two mass loss extreme values, and similar trend can be found in the previous literature (Liu et al., 2019).

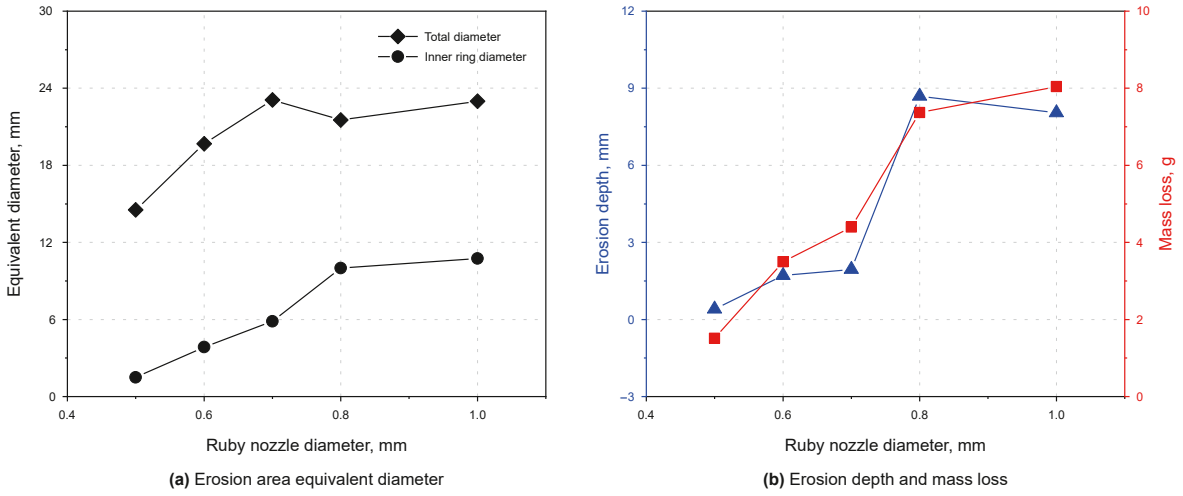

Fig. 8. Rock-breaking performance at different ruby nozzle diameters.

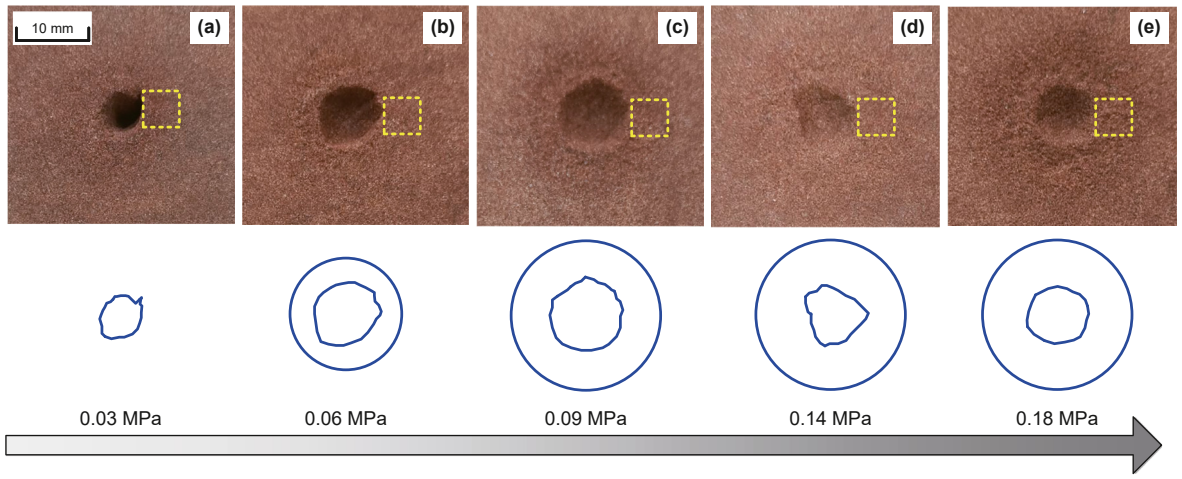

Fig. 9. Erosion hole appearance at different low-speed waterjet pressures.

To investigate the effect of low-speed waterjet pressure on cavitation erosion. As shown in Fig. 11, the areas eroded by the cavitation bubble on the sandstone surface are shown by the 3D profiler and the scanned position is boxed in Fig. 9. As mentioned above, no obvious cavitation areas are observed with relatively smooth surface profiles and a maximum depth of about 250 μm, shown in Fig. 11(a). As shown in Fig. 11(b), deeper erosion areas are obtained on the sandstone surface, with a maximum depth of around 300 μm. When the pressure is greater than 0.09 MPa, more obvious erosion pits appear on the sandstone surface, the area eroded by the collapse of cavitation bubbles increases in size, with a maximum depth of 500 μm or more.

To quantify and characterize the cavitation eroded areas, the roughness of the cavitation erosion area is measured with the help of a 3D profiler. As shown in Fig. 12, the roughness of the area eroded by cavitation bubbles increases with the increasing pressure of the low-speed waterjet. The surface roughness is only 22.7 μm at low-speed waterjet pressure of 0.03 MPa, but increases to 134 μm when the low-speed waterjet pressure is 0.18 MPa. This indicates that the cavitation bubble collapse intensity increases with the increase of low-speed waterjet pressure, which allows more sandstone particles to be exfoliated.

To further elucidate the reasons for the variation of cavitation erosion intensity on the sandstone surface, transient pictures of UCAWJ at different low-speed waterjet pressures were observed. When the low-speed waterjet pressure is 0.03 MPa, part of the cavitation bubbles collapse due to air contact before reaching the sandstone surface. As shown in Fig. 13(a(i)), at moment T_0, due to the suction of the high-speed waterjet, the low-speed waterjet is displaced radially, resulting in cavitation bubbles in contact with the air. At moment T_0+2 ms, the energy generated by the collapse of the cavitation bubble makes the water splash into the air, and a similar trend was observed in Fig. 13(b). The contact between cavitation bubbles and air was also obtained at low-speed waterjet pressures of 0.06 MPa. However, with the increase of the low-speed waterjet pressure, the squeezing pressure on the cavitation bubble becomes larger, and it is difficult for the cavitation bubble to move to the boundary of the waterjet and contact with the air at low-speed waterjet pressure of 0.09, 0.14 and 0.18 MPa, respectively. In conclusion, when the low-speed waterjet pressure is small, the cavitation bubbles easily reach the boundary of the waterjet and contact with air, the erosion of the sandstone surface by the cavitation bubbles is reduced. At low-speed waterjet pressures greater than 0.09 MPa, shear cavitation bubbles collapse with increased

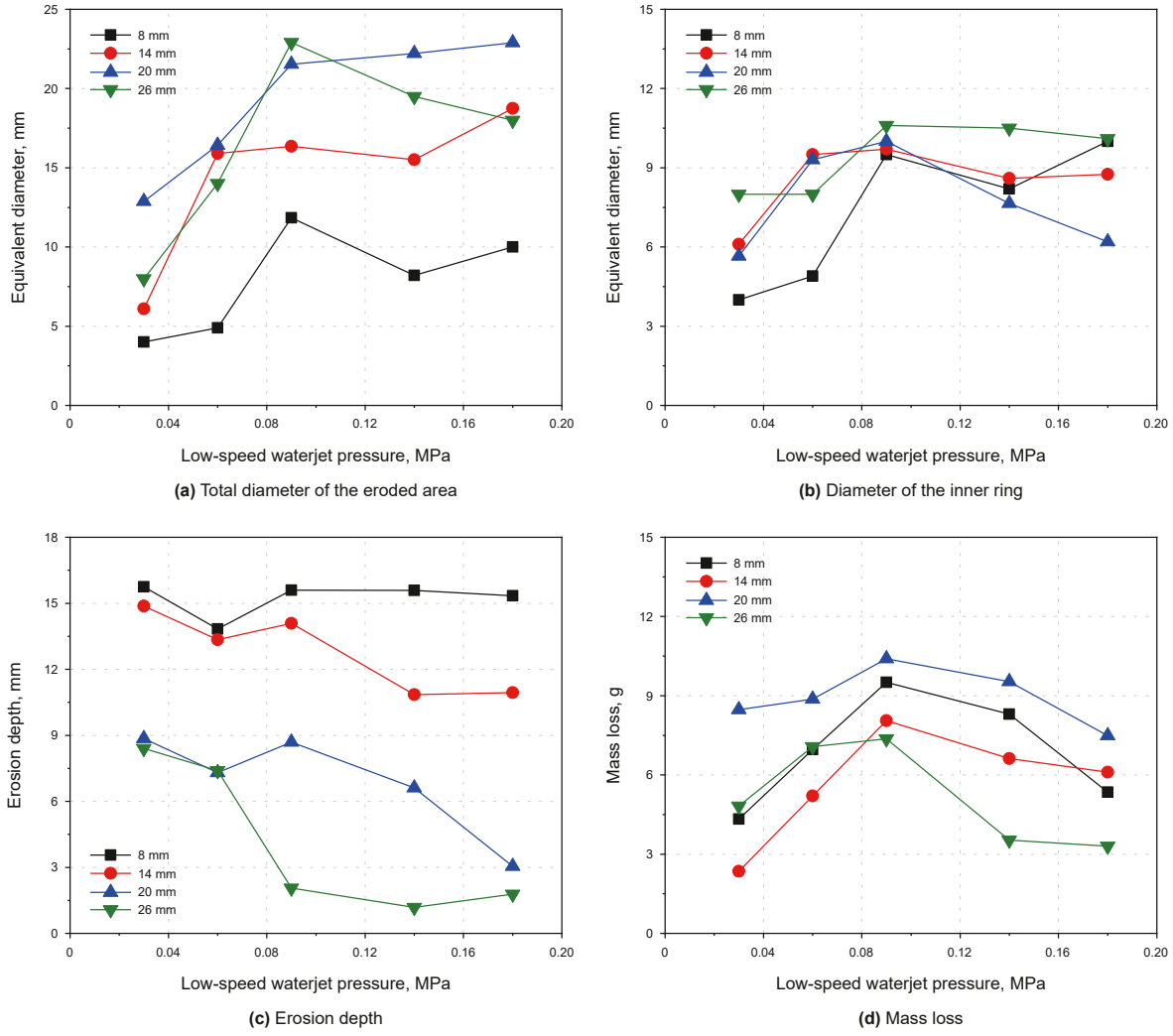

Fig. 10. Rock-breaking performance varies with low-speed waterjet pressure at different standoff distances.

intensity, which allows more sandstone to be eroded. However, as the pressure of the low-speed waterjet increases, the high-speed waterjet is observed to become lighter in color. This indicates a decrease in the velocity gradient between the jets, causing a reduced generation of cavitation bubbles, a phenomenon that has been described above. Meanwhile, due to the increased restraint of the low-speed waterjet, the momentum decay of the high-speed waterjet is allowed to be more rapid, which reduces the erosion ability of the high-speed waterjet, a phenomenon that corresponds to Figs. 10 and 11(c).

In addition, based on previous studies (Long et al., 2017; Sarc et al., 2017), the higher the pressure of the low-speed waterjet, the corresponding increase in the cavitation number and the weakening of the cavitation phenomenon. In general, the weaker the cavitation phenomenon, the less erosion. But in the present study, a different trend is observed. The possible reason for this is that although more obvious cavitation bubble occurs, the increased intensity of cavitation bubble collapse is not confirmed. When a smaller low-speed waterjet pressure, the cavitation bubble collapse is weaker due to the lower compression pressure of the external flow field on the cavitation bubble, which can be found in previous studies to explain (Peng et al., 2017). With the increase of low-speed waterjet pressure, the cavitation bubble collapse intensity increases and causes deeper erosion pits on the sandstone surface, which is also well confirmed by Figs. 11 and 12. However, when the low-speed waterjet pressure is too high, it leads to insufficient development of cavitation bubbles, which results in weaker collapse intensity. While in this paper, due to the limitation of equipment parameters, the optimal low-speed waterjet pressure has not been sought to make the maximum cavitation intensity.

3.3. Sandstone damage mechanism of UCAWJ

Based on the above mentioned, the erosion area of sandstone can be divided into two parts, shown in Fig. 14. The first part is the outer ring, which is mainly caused by erosion when shear cavitation bubbles collapse on the surfaces of sandstone. The second is the inner hole, which is mainly caused by the erosion of high-speed abrasive waterjet. Furthermore, the inner ring can also be divided into two types under different working conditions. The first when the erosion hole is shallow and the second when it is deep, both of which have slightly different mechanisms when the sandstone is damaged by erosion, as will be described in detail later.

In the outer ring of the erosion zone, pressure waves, transient high temperatures and microjets generated by shear cavitation collapse resulted in the dislodging of sandstone particles, and significant uneven erosion pits were observed in the outer ring. At the same time, the abrasive particles will also erode the outer ring

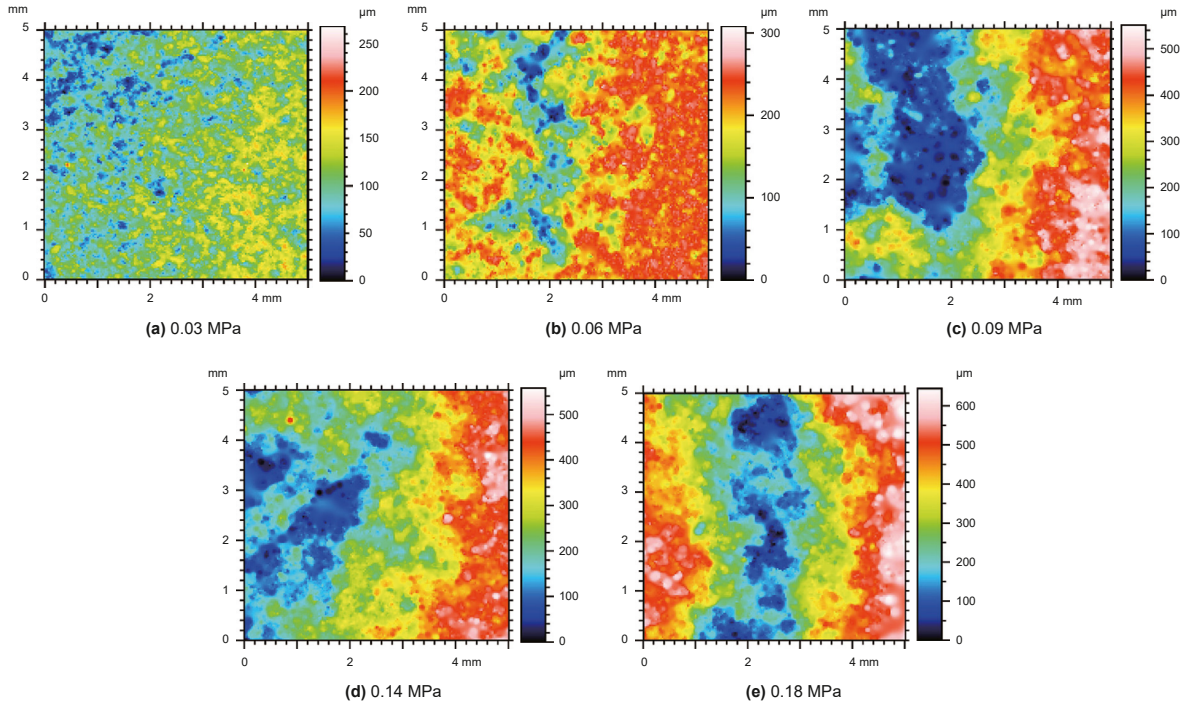

Fig. 11. Surface profile of cavitation erosion area at different low-speed waterjet pressures.

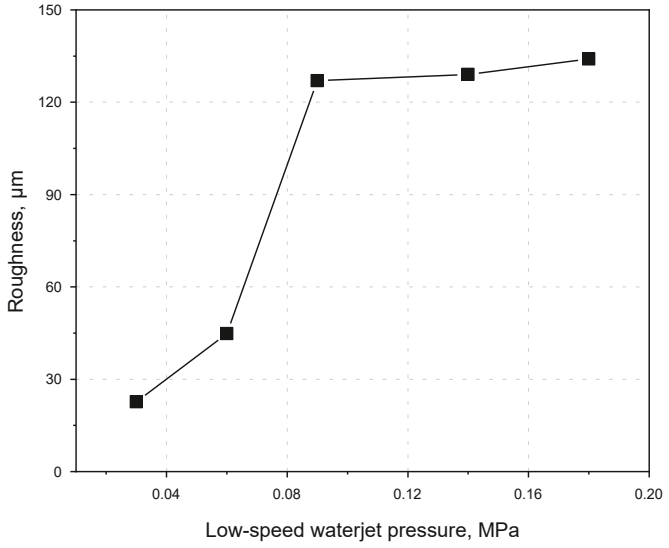

Fig. 12. Surface roughness of cavitation erosion area at different low-speed waterjet pressures.

during the external movement, but the erosion effect is much weaker than the collapse of cavitation bubbles. For the erosion holes in the inner, when the erosion hole is shallow, a regular and smooth hole is obtained on the sandstone surface due to the uniform distribution of abrasives and the polishing effect of abrasives (Haj Mohammad Jafar et al., 2015). However, there is a difference when the erosion hole is deeper, abrasive particles cannot be discharged from the erosion hole in time, and the second bounce of the abrasive particles will also occur in the space of the erosion hole. The collapse of cavitation bubble not only erodes the sandstone, but also accelerates the abrasive particles. Thus, the kinetic energy of abrasive particles increases, which intensifies the erosion, causing more sandstone particles to be dislodged, which further enlarges the erosion hole.

Fig. 15 shows SEM images of the three locations of the erosion holes under the impact of the UCAWJ. The outer ring of the erosion area is shown in Fig. 15(a), the mineral grains are relatively intact, but the cement between the mineral grains is destroyed, obvious micro-pores and micro-cracks are observed. Furthermore, the surface of mineral particles is broken into tiny rock fragments, mostly flake rock fragments and wedge-shaped rock fragments shown in Figs. 15(a-2). Sandstone is a typical polycrystalline material, by observing the microscopic morphology of the erosion surface. As shown in Fig. 15(b), it can be found that sandstone is fractured along the grain boundary and fracture through the grain, the fracture through the grain is predominant, and similar patterns can be found in previous studies (Liu et al., 2021; Zhang et al., 2021). Under the transient impact of the abrasive particles and the fluid-water wedge pressure, the tightly cemented connection between the mineral particles and the matrix in the sandstone is destroyed. Causes shear or tensile damage along primary cracks within mineral particles or at a lower strength, micro-cavity and micro-fractures can be observed. In addition, the cutting effect of abrasive particles is evident, mineral particles are broken into numerous rock chips, obvious mineral particle fractures are obtained and shown in Figs. 15(b-2). The inner wall of the erosion hole is further eroded by the secondary rebound of the abrasive particles, but the erosion ability of the abrasive particles is weaker due to the water buffer. As shown in Figs. 15(c-1), the cement of the mineral particles is also destroyed, accompanied by smoother edges and a small number of abrasive cuts on the edges of the mineral grains. Interestingly, on the surface of the mineral grains, honeycomb monazite appears and there is no obvious trace of erosion. This also indicates the weak erosion ability of the secondary rebound abrasive particles, the high turbulence within the erosion holes also resulted in the free dislodgement of mineral particles.

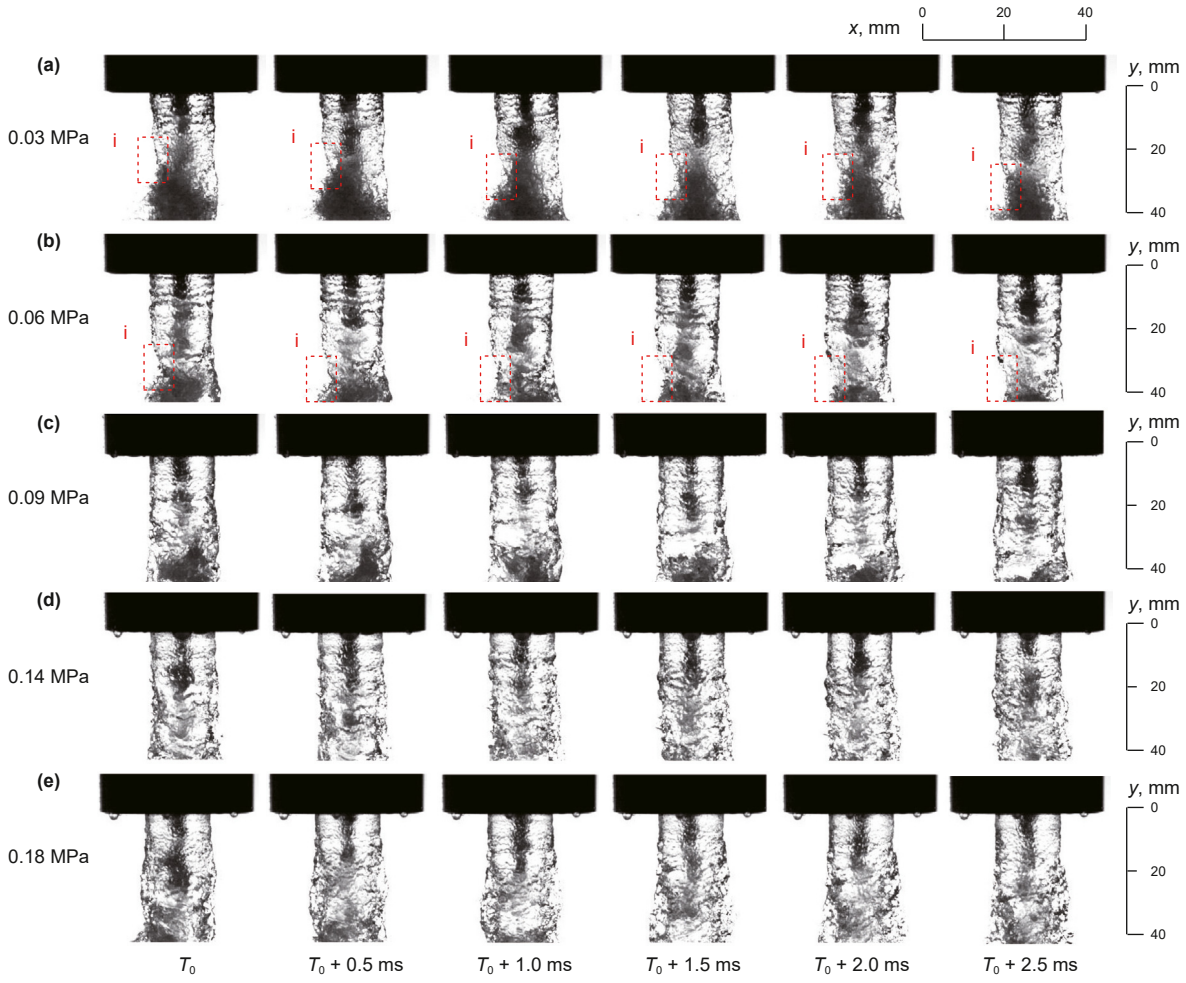

Fig. 13. Transient pictures of UCAWJ at different low-speed waterjet pressures.

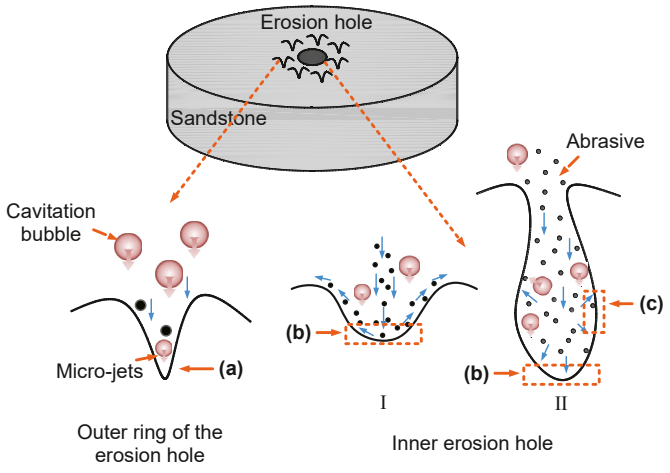

Fig. 14. Rock-breaking mechanism of UCAWJ.

4. Conclusion

This paper presented an experimental study of the effect of low-speed waterjet pressure on the rock-breaking performance of UCAWJ. Measurements of sandstone erosion holes are made to assess the rock-breaking performance, a combination of high-speed photography and three-dimensional profilometry was used to illustrate the effect of low-speed waterjet pressure on cavitation intensity. The following conclusions can be drawn from the analysis of the results.

(1) The appearance of the inner ring erosion holes is regular and close to circular, the rock-breaking performance increases nearly linearly with erosion time. When the ruby nozzle is larger than 0.6 mm, a more obvious cavitation erosion area can be obtained.
(2) The mass loss of sandstone increases first and then decreases with the increase of low-speed waterjet pressure, the maximum mass loss of 10.4 g is obtained at pressure of 0.09 MPa and standoff distance of 20 mm.
(3) By observation and measurement of the cavitation erosion area, the increase in low-speed waterjet pressure enhances the cavitation bubble collapse intensity. The maximum erosion depth of cavitation bubble collapse on the sandstone surface is 600 μm with a roughness of 127 μm at low-speed waterjet pressure of 0.18 MPa.
(4) The inner erosion hole is dominated by crystal penetration fracture, the mineral particles in the inner wall of the erosion hole are dominated by free detachment, for the cavitation erosion, the cement between the mineral particles is obviously destroyed.

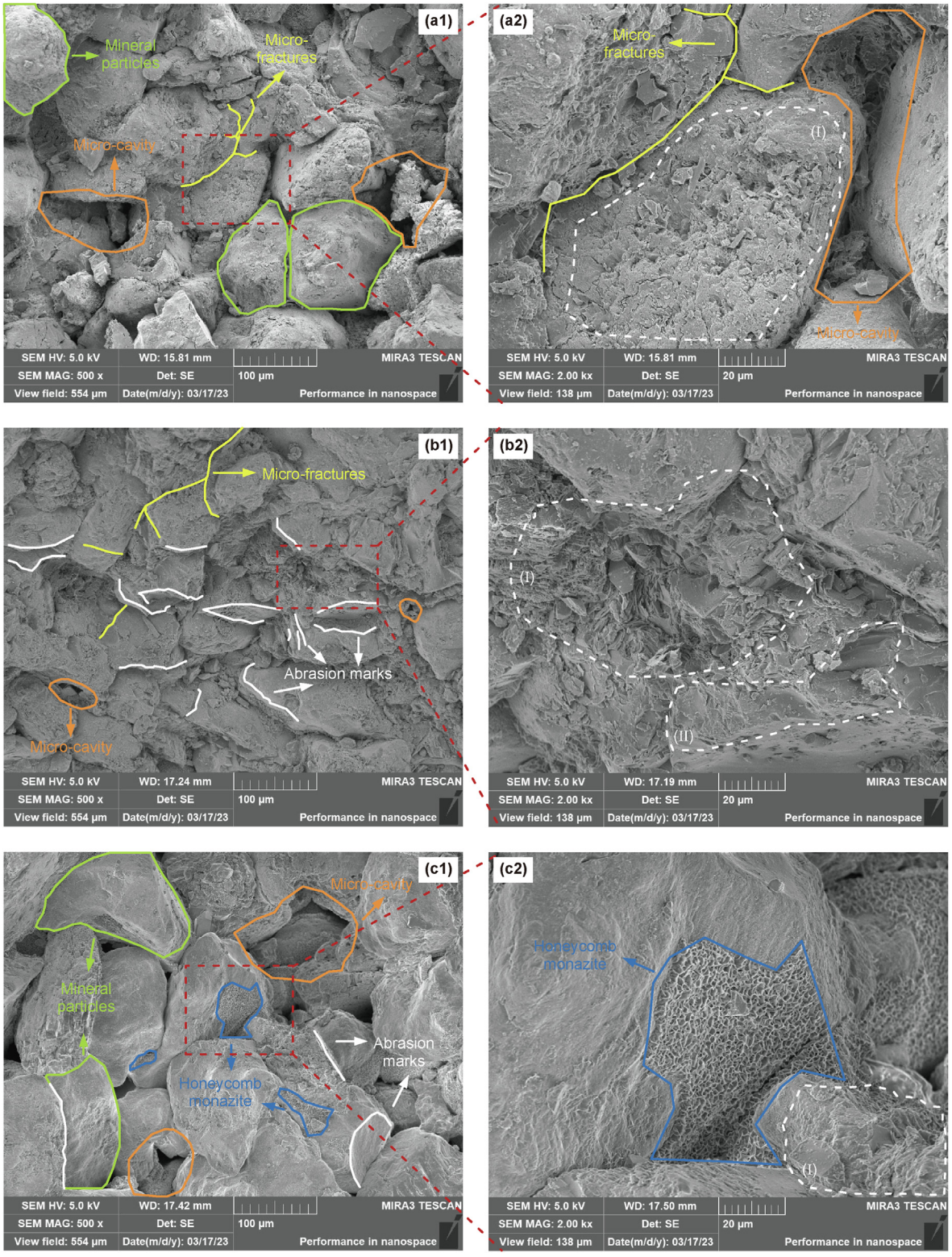

Fig. 15. SEM images at (**a**) the outer ring erosion hole, (**b**) the bottom and (**c**) the sidewall of the inner ring erosion hole.

Conflict of interest

The authors declare that they have no known competing financial interests or personal relationships that could have appeared to influence the work reported in this paper.

CRediT authorship contribution statement

Chen-Xing Fan: Writing – original draft, Visualization, Methodology, Investigation, Formal analysis, Data curation, Conceptualization. **Deng Li:** Writing – review & editing, Visualization,

Validation, Project administration, Funding acquisition. **Yong Kang:** Writing – review & editing, Visualization, Validation, Project administration, Funding acquisition. **Hai-Tao Zhang:** Supervision, Software, Resources, Investigation.

Acknowledgements

This research is financially supported by the National Natural Science Foundation of China (Nos. 52175245 and 52274093), the Natural Science Foundation of Hubei Province (No. 2021CFB462) and the Knowledge Innovation Special Project of Wuhan (whkxjsj007).

References

Bruno Arab, P., Barreto Celestino, T., 2020. A microscopic study on kerfs in rocks subjected to abrasive waterjet cutting. Wear 448–449. https://doi.org/10.1016/j.wear.2020.203210.

Cai, T.F., Pan, Y., Ma, F., et al., 2021. Effects of ambient pressure on the frequency characteristics of self-excited cavitating waterjet. Ocean. Eng. 237, 109623. https://doi.org/10.1016/j.oceaneng.2021.109623.

Cha, Y., Oh, T.M., Joo, G.W., et al., 2021. Performance and reuse of steel shot in abrasive waterjet cutting of granite. Rock Mech. Rock Eng. 54 (3), 1551–1563. https://doi.org/10.1007/s00603-020-02332-8.

Ge, Z.L., Shangguan, J.M., Zhou, Z., et al., 2023. Investigation of fracture damage and breaking energy consumption of hard rock repeatedly cut by abrasive water jet. Rock Mech. Rock Eng. 56 (4), 3215–3230. https://doi.org/10.1007/s00603-023-03230-5.

Grosso, B., Dentoni, V., Bortolussi, A., 2021. Effect of the rock stress on the water jet cutting performance. Rock Mech. Rock Eng. 54 (9), 4987–4999. https://doi.org/10.1007/s00603-021-02508-w.

Guo, C., Lin, B.Q., Yao, H., et al., 2019. Characteristics of breaking coal-rock by submerged jet and its application on enhanced coal bed methane recovery. Energy. Sources. Part. A: recovery. Utilization, and Environmental Effects 42 (18), 2249–2260. https://doi.org/10.1080/15567036.2019.1607937.

Haj Mohammad Jafar, R., Nouraei, H., Emamifar, M., et al., 2015. Erosion modeling in abrasive slurry jet micro-machining of brittle materials. J. Manuf. Process. 17, 127–140. https://doi.org/10.1016/j.jmapro.2014.08.006.

Hutli, E., Nedeljkovic, M.S., Radovic, N.A., et al., 2016. The relation between the high speed submerged cavitating jet behaviour and the cavitation erosion process. Int. J. Multiphas. Flow 83, 27–38. https://doi.org/10.1016/j.ijmultiphaseflow.2016.03.005.

Liu, B.S., Pan, Y., Ma, F., 2019. Pulse pressure loading and erosion pattern of cavitating jet. Engineering Applications of Computational Fluid mechanics 14 (1), 136–150. https://doi.org/10.1080/19942060.2019.1695675.

Liu, J.L., Zhu, Y.J., Xue, Y.Z., et al., 2021. Fragmentation pattern and removal mechanism of concrete subjected to abrasive water jet impact. Adv. Mater. Sci. Eng. 2021, 1–10. https://doi.org/10.1155/2021/6618386.

Liu, S.Y., Zhou, F.Y., Li, H.S., et al., 2020. Experimental investigation of hard rock breaking using a conical pick assisted by abrasive water Jet. Rock Mech. Rock Eng. 53 (9), 4221–4230. https://doi.org/10.1007/s00603-020-02168-2.

Long, X.P., Zhang, J.Q., Wang, J., et al., 2017. Experimental investigation of the global cavitation dynamic behavior in a venturi tube with special emphasis on the cavity length variation. Int. J. Multiphas. Flow 89, 290–298. https://doi.org/10.1016/j.ijmultiphaseflow.2016.11.004.

Lu, Y.Y., Huang, F., Liu, X.C., et al., 2015. On the failure pattern of sandstone impacted by high-velocity water jet. Int. J. Impact Eng. 76, 67–74. https://doi.org/10.1016/j.ijimpeng.2014.09.008.

Lv, L., Zhang, Y.X., Zhang, Y.N., et al., 2019. Experimental investigations of the particle motions induced by a laser-generated cavitation bubble. Ultrason. Sonochem. 56, 63–76. https://doi.org/10.1016/j.ultsonch.2019.03.019.

Marcon, A., Melkote, S.N., Castle, J., et al., 2016. Effect of jet velocity in co-flow water cavitation jet peening. Wear 360–361, 38–50. https://doi.org/10.1016/j.wear.2016.03.027.

Marcon, A., Melkote, S.N., Yoda, M., 2018. Effect of nozzle size scaling in co-flow water cavitation jet peening. J. Manuf. Process. 31, 372–381. https://doi.org/10.1016/j.jmapro.2017.12.002.

Pan, Y., Ji, S.M., Tan, D.P., et al., 2020a. Cavitation-based soft abrasive flow processing method. Int. J. Adv. Manuf. Technol. 109 (9–12), 2587–2602. https://doi.org/10.1007/s00170-020-05836-3.

Pan, Y., Ma, F., Liu, B.S., et al., 2020b. Cavitation intensity and erosion pattern of a self-excited cavitating jet. J. Mater. Process. Technol. 282, 116668. https://doi.org/10.1016/j.jmatprotec.2020.116668.

Peng, C., Tian, S.C., Li, G.S., 2018. Joint experiments of cavitation jet: high-speed visualization and erosion test. Ocean. Eng. 149, 1–13. https://doi.org/10.1016/j.oceaneng.2017.11.009.

Peng, K.W., Tian, S.C., Li, G.S., et al., 2018. Mapping cavitation impact field in a submerged cavitating jet. Wear 396–397, 22–33. https://doi.org/10.1016/j.wear.2017.11.006.

Peng, K.W., Tian, S.C., Li, G.S., et al., 2017. Cavitation in water jet under high ambient pressure conditions. Exp. Therm. Fluid Sci. 89, 9–18. https://doi.org/10.1016/j.expthermflusci.2017.07.021.

Sarc, A., Stepisnik-Perdih, T., Petkovsek, M., et al., 2017. The issue of cavitation number value in studies of water treatment by hydrodynamic cavitation. Ultrason. Sonochem. 34, 51–59. https://doi.org/10.1016/j.ultsonch.2016.05.020.

Soyama, H., 2007. Improvement of fatigue strength by using cavitating jets in air and water. J. Mater. Sci. 42 (16), 6638–6641. https://doi.org/10.1007/s10853-007-1535-8.

Soyama, H., 2020. Cavitating jet: a review. Appl. Sci. 10 (20), 7280. https://doi.org/10.3390/app10207280.

Soyama, H., Kikuchi, T., Nishikawa, M., et al., 2011. Introduction of compressive residual stress into stainless steel by employing a cavitating jet in air. Surf. Coating. Technol. 205 (10), 3167–3174. https://doi.org/10.1016/j.surfcoat.2010.11.031.

Wang, F.C., Zhou, D.P., Xu, Q.W., et al., 2018. Mathematical model of rock stress under abrasive slurry jet impact based on contact mechanics. Int. J. Rock Mech. Min. Sci. 107, 1–8. https://doi.org/10.1016/j.ijrmms.2018.04.010.

Watanabe, R., Yanagisawa, K., Yamagata, T., et al., 2016. Simultaneous shadowgraph imaging and acceleration pulse measurement of cavitating jet. Wear 358–359, 72–79. https://doi.org/10.1016/j.wear.2016.03.036.

Xue, Y.Z., Si, H., Xu, D.Y., et al., 2018. Experiments on the microscopic damage of coal induced by pure water jets and abrasive water jets. Powder Technol. 332, 139–149. https://doi.org/10.1016/j.powtec.2018.03.051.

Zelenak, M., Riha, Z., Votavova, H., et al., 2022. Methods for the behaviour analysis of continuous flat water jet structures. Measurement 202, 111886. https://doi.org/10.1016/j.measurement.2022.111886.

Zhang, M.D., Li, D., Kang, Y., et al., 2021. Experimental study on the rock erosion performance of a pulsed abrasive supercritical CO_2 jet. J. Petrol. Sci. Eng. 201, 108489. https://doi.org/10.1016/j.petrol.2021.108489.

Zhang, Y.Q., Zhao, K.X., Wu, X.Y., et al., 2020. An innovative experimental apparatus for the analysis of natural gas hydrate erosion process using cavitating jet. Rev. Sci. Instrum. 91 (9), 095107. https://doi.org/10.1063/5.0011951.

Zheng, H.X., Luo, Y., Zang, J.Y., et al., 2022. Effect of nozzle outlet type on the flow field velocity and impact pressure of high-pressure water jet peening. Journal of Fluids Engineering-transactions of The Asme 144 (7), 1–10. https://doi.org/10.1115/1.4053446.